ISSN 1063-7729, Astronomy Reports, 2009, Vol. 53, No. 1, pp. 86–94. © Pleiades Publishing, Ltd., 2009.
Original Russian Text © D.P. Barsukov, P.I. Polyakova, A.I. Tsygan, 2009, published in Astronomicheskiĭ Zhurnal, 2009, Vol. 86, No. 1, pp. 95–104.

Effect of the Pulsar-Tube Radius on the Gamma-Ray Curvature Radiation from the Polar Regions of Radio Pulsars with Non-Dipolar Magnetic Fields

D. P. Barsukov, P. I. Polyakova, and A. I. Tsygan

Ioffe Physical–Technical Institute, Russian Academy of Sciences, ul. Politekhnicheskaya 26, St. Petersburg, 194021 Russia

Received June 11, 2008; in final form, July 2, 2008

Abstract—The effect of the radius of the tube of open magnetic-field lines on the gamma-ray curvature radiation from the polar regions of a radio pulsar with a non-dipolar magnetic field is analyzed. The pulsar is considered in a polar-cap model with free electron emission from the neutron-star surface. The effect of the non-dipolar magnetic field on the radius of curvature of the field lines and the field intensity is taken into account. In connection with the creation of electron–positron pairs, we take into account only the birth of pairs by curvature radiation in the magnetic field. The small non-dipolarity of the field enables the radio pulsar not to turn off, even after a considerable decrease in the pulsar-tube radius. For instance, with a 20% non-dipolarity ($\nu = 0.2$), a pulsar with $B = 10^{13}$ G and $P = 0.5$ s can still operate even for a fivefold decrease in the pulsar-tube radius. A maximum is observed in the dependence of the electrostatic potential in the diode on the non-dipolarity parameter ν at $\nu \sim 0.5$–0.7. The pulse profile in non-thermal X-ray emission for $\nu \sim 0.5$–0.7 may look virtually the same as for $\nu \sim 0.1$–0.2. Decreases in the pulsar-tube radius could be due to a structure of currents in the magnetosphere that results in the pulsar diode on the neutron-star surface occupying only a small fraction of the pulsar tube, with the remainder of the tube containing an outer annular gap. The pulsar-tube size is also affected by the presence of a circum-pulsar disk. A change in the pulsar-tube radius could also be due to an external magnetic field, associated with either a magnetic white dwarf or a circum-pulsar disk.

PACS numbers: 97.60.Gb
DOI: 10.1134/S1063772909010107

1. INTRODUCTION

The global structures of pulsar magnetospheres are currently being actively studied (see, e.g., [1–3]). The most important region in the magnetosphere is the region with open magnetic-field lines (the pulsar tube), where the radio and gamma-ray radiation of the pulsar are generated. Even small changes in the structure of the magnetosphere can strongly influence the gamma-ray and X-ray radiation of the pulsar, as well as its radio emission [3, 4].

The presence of small-scale magnetic fields near the neutron-star surface is no less important for the pulsar tube's operation. These fields also give rise to appreciable changes in the non-thermal X-ray and gamma-ray radiation of the pulsar tube.

The X-ray and gamma-ray radiation of pulsars in the absence of small-scale magnetic fields and distortions in the outer part of the pulsar magnetosphere has been studied in detail in many works (see, e.g., [5–9]). The possible existence of small-scale magnetic fields and their effect on the operation of the pulsar was considered in [5, 10–14].

The current paper is a direct follow-up of [15–18]. We consider here only one aspect of distortions in the pulsar magnetosphere: the effect of the pulsar-tube radius on the non-thermal X-ray and gamma-ray radiation of the pulsar. We allow for the possible existence of small-scale magnetic fields near the neutron-star surface.

We considered the radio pulsar in a Goldreich–Julian model (a "polar cap" model) with the free emission of electrons from the neutron-star surface. Near the surface, there is a region with a non-zero longitudinal electric field ($E_{||} = \mathbf{EB}/B \neq 0$), called the pulsar diode [19].

When calculating the intensity of the non-thermal X-ray and gamma-ray radiation of the pulsar tube, we considered only the curvature radiation of primary electrons. This approximation is justified at energies up to 100 MeV if the surface temperature of the neutron star and polar cap is fairly low, $T < 10^6$ K.

We also neglect all general relativistic effects except for the dragging of inertial reference frames,

which makes an important contribution to the electrostatic potential.

2. ELECTRIC FIELD

We describe the non-dipolarity of the magnetic field near the neutron-star surface using the same model as in [16] (see also [17, 18]). Thus, the magnetic field near the neutron-star surface (with radius we denote a) is described using two dipoles. The first dipole (the main one, with the greatest magnitude) $\mathbf{m}$ is at the center of the neutron star. We denote the angle between $\mathbf{m}$ and the pulsar rotation axis $\mathbf{\Omega}$ χ, and will assume everywhere that $\chi = 10°$. The second dipole, $\mathbf{m}_1$, is located in the region of the magnetic pole of the neutron star (with its center on the axis of the main dipole $\mathbf{m}$) at a distance $a\Delta$ from the surface (deep in the star). We will take $\mathbf{m}_1$ to be perpendicular to $\mathbf{m}$; the angle between $\mathbf{m}_1$) and the $(\mathbf{m}, \mathbf{\Omega})$ plane is denoted γ ($\gamma = \pi$ corresponds to $\mathbf{m}_1$ lying in the $(\mathbf{m}, \mathbf{\Omega})$ plane and directed toward the pulsar rotation axis). We will assume everywhere $\Delta = 0.1$.

Let us introduce a spherical coordinate system $(\eta = \dfrac{r}{a}, \theta, \phi)$ s with its origin at the neutron-star center $\eta = 0$; we align the Oz axis with $\mathbf{m}$ and the Ox axis with $\mathbf{m}_1$; thus, $\mathbf{m} = m\mathbf{e}_z$ and $\mathbf{m}_1 = m_1\mathbf{e}_x$. In this coordinate system, in the small-angle approximation $\theta \ll 1$, the magnetic field near the neutron-star surface is [16]

$$B_r = \frac{B_0}{\eta^3}, \quad B_\theta = \frac{B_0}{\eta^3}\left(\frac{\theta}{2} + \mu\cos\phi\right), \qquad (1)$$
$$B_\phi = -\frac{B_0}{\eta^3}\mu\sin\phi,$$

where $\mu = \nu\left(\dfrac{\Delta\eta}{\eta - 1 + \Delta}\right)^3$, $\nu = B_1/B_0$, and B_0 and B_1 are the magnetic-field intensities created by the dipoles $\mathbf{m}$ and $\mathbf{m}_1$, respectively, at the magnetic pole of the neutron star ($\eta = 1, \theta = 0, \phi = 0$).

To find the curvature of the magnetic-field lines we use formula (2) from [16] (see also [18]):

$$\rho_c = 2\eta a\left\{\frac{3}{2}\theta + \mu\left[\left(\frac{3(1-\Delta)}{\eta - 1 + \Delta}\right) - \frac{1}{2}\right]\right\}^{-1}. \quad (2)$$

We can find the electric field in the pulsar tube using the model described in [17] (the notation we use here is described in [18]). In the case of a thin pulsar tube (when the height of the upper plate of the diode $z_c = \eta_c - 1$ is much greater than the pulsar-tube radius θ_s), the electric potential in the pulsar diode is calculated using formula (10) from [17]:

$$\Phi = \frac{\Omega F}{2\pi c}(1 - \xi^2) \qquad (3)$$
$$\times\left[\left(1 - \frac{k}{\eta^3}\right)f(\eta) - (1-k)f(1)\right],$$

where

$$f(\eta) = (\cos\chi + \mu\sin\chi\cos\gamma)\frac{1}{\sqrt{1+\mu^2}},$$

where F is the magnetic flux through the pulsar tube, and ξ is the distance across the tube ($\xi = 1$ corresponds to the tube boundary and $\xi = 0$ to the central magnetic-field line).

In this case, according to formula (8) of [17], the electric charge density is

$$\rho(\eta, \xi, \phi) = \frac{\Omega B}{2\pi c}(1-k)f(1), \qquad (4)$$

where B is the magnetic-field intensity at the point (η, ξ, ϕ).

If $z_c \ll 1$, $z_c \ll \Delta$, $\theta \ll 1$, and $\sin\beta \ll \dfrac{\theta_s}{z_c}$ or $\dfrac{z_c}{\theta_s}$, where β is the angle between the magnetic field $\mathbf{B}$ and the normal to the neutron-star surface $\mathbf{e}_r$, we can find the electrostatic potential in the region of the pulsar diode using formula (6) of [18]:

$$\Phi = 2\Phi_0\, K_1 \sum_{i=1}^{\infty}\frac{1}{\gamma_i^2}\left(z + \frac{F(z,\gamma_i)}{\gamma_i}\right) \qquad (5)$$
$$\times\frac{2}{k_i J_1(k_i)}J_0(k_i\xi),$$

where

$$F(z,\gamma) = -\frac{(1 - e^{-\gamma z})\left(1 + e^{-\gamma(z_c - z)}\right)}{1 + e^{-\gamma z_c}},$$

where $\Phi_0 = \dfrac{\Omega a}{c}B_s a$, $\gamma_i = \dfrac{k_i}{\theta_s}$, k_i are the roots of the equation $J_0(k) = 0$, B_s is the magnetic-field intensity at the neutron-star surface at the center of the pulsar tube ($\eta = 1$, $\xi = 0$, $\phi = 0$), and $\theta_s a$ is the pulsar-tube radius at the neutron-star surface. Due to the conservation of magnetic flux in the tube, $\theta_s^2 a^2 B_{sur}^2 = F$.

The expressions for the coefficients K_0 and K_1 are

$$K_0 = \frac{1}{\sqrt{1+\nu^2}}\left[(1-k)\cos\chi + \left(1 + \frac{k}{2}\right)\nu\sin\chi\cos\gamma\right],$$

$$K_1 = \frac{1}{\sqrt{1+\nu^2}}\left[3k + \frac{3\nu}{\Delta}\frac{\nu}{1+\nu^2}(1-\Delta) \times (1-k)\right]\cos\chi,$$

$$-\frac{3\nu}{\Delta}\frac{1}{(1+\nu^2)^{3/2}}\left(1 - \Delta + \frac{k}{2} + \frac{k}{2}\nu^2\Delta\right)\sin\chi\cos\gamma.$$

In this case, we can find the electric charge density in the region of the pulsar diode using formula (4) of [20]:

$$\rho(\eta,\xi,\phi)=\frac{\Omega B}{2\pi c}A(\xi),$$

$$A(\xi)=-K_0-K_1\sum_{i=0}^{\infty}\frac{1}{\gamma_i}\frac{1-e^{-\gamma_i z_c}}{1+e^{-\gamma_i z_c}}\frac{2}{k_i J_1(k_i)}J_0(k_i\xi),$$

where B is the magnetic-field intensity at the point (η,ξ,ϕ).

In the region $0\le z\le z_c$ (the region of the pulsar diode), we assume the energy of the primary electrons to be

$$E(\eta,\xi,\phi)\equiv mc^2\Gamma(\eta,\xi,\phi)=e\Phi mc^2,$$

where Φ is the electrostatic potential at (η,ξ,ϕ).

When radiative deceleration is taken into account, we can find the energy of the primary electrons in the screening region $z\ge z_c$ using formula (3) of [15]:

$$\Gamma(z,\xi,\phi)=\frac{\Gamma_c}{\left[1+\frac{9}{8}\frac{r_e}{a}\theta_0^2\xi^2\Gamma_c^3\ln\left(\frac{\eta}{\eta_c}\right)\right]^{1/3}},$$

where we have denoted $\Gamma_c=\dfrac{e\Phi}{mc^2}(z_c,\xi,\phi)$ and $r_e=\dfrac{e^2}{mc^2}$ is the classic electron radius. If radiative deceleration is neglected, we assume for the energy of the primary electrons at $z\ge z_c$ $\Gamma(\eta,\xi,\phi)=\Gamma_c$.

The height of the upper plate z_c of the pulsar diode is chosen precisely as in [20] (see also [18]); i.e., it is assumed that, at the point $(z=z_c,\ \xi=\dfrac{1}{2},\ \phi=0)$ (which is shifted from the pulsar-tube center toward positive values of x, i.e., in the direction of $\mathbf{m}_1$), the electron–positron pair multiplication factor is

$$Q\left(z=z_c,\xi=\frac{1}{2},\phi=0\right)=0.1. \qquad (6)$$

When calculating Q, we considered only the generation of electron–positron pairs via the absorption of curvature photons radiated by primary electrons in the magnetic field.

The generation of gamma-ray radiation is calculated precisely as in [18]. We took into account only curvature radiation of the primary electrons and its absorption in the magnetic field (leading to the birth of electron–positron pairs).

3. CHANGE IN THE TUBE RADIUS

We considered only the distortion in the pulsar magnetosphere in the form of changes in the pulsar-tube radius. When calculating the electron–positron pair multiplication coefficient Q and the gamma-ray intensity, we took the magnetic field at large heights to be purely dipolar (coincident with the field of the main dipole $\mathbf{m}$), and neglected the shift of the pulsar-tube center relative to the axis of the main dipole $\mathbf{m}$ at large heights. Moreover, we assumed throughout that the pulsar-tube cross section is circular, and that the pulsar-tube radius at large heights is given by $d\theta_{0\mathrm{dip}}a\eta^{\frac{3}{2}}$, where $\theta_{0\mathrm{dip}}=\sqrt{\dfrac{\Omega a}{c}}$. The magnetic flux F through the pulsar tube was taken to be

$$F=B_0\pi\theta_{0\mathrm{dip}}^2d^2a^2,$$

where the dimensionless parameter d describes the decrease in the pulsar-tube radius relative to its purely dipolar value $\theta_{0\mathrm{dip}}$: $\theta_0=d\theta_{0\mathrm{dip}}$.

Generally speaking, finding the pulsar-tube radius allowing for all currents flowing in the magnetosphere and for possible external disturbances is a complicated and, until now, not fully solved, problem (see, e.g., [2, 21]). Therefore, we treat d as, generally speaking, arbitrarily chosen model parameter.

One interesting case is when the current through the pulsar tube flows such that the standard pulsar diode can exist at the neutron-star surface only in a small region near the pulsar-tube center, while the remainder of the tube is occupied by an annular gap [22]. As a result, in spite of the fact that the tube radius may remain constant, the diode at the neutron-star surface operates as if the tube radius has strongly decreased. Note that Timokhin [1] obtained a current distribution in the pulsar tube very similar to that described in [22].

In the case of an external influence on the magnetosphere of a radio pulsar, the value of d can be estimated as follows. If the pulsar is surrounded by a circum-pulsar disk, its interaction with the pulsar magnetosphere can result in the appearance of electric currents that, in some situations, can change the entire structure of the magnetosphere and, as a minimum, the pulsar-tube radius (see, e.g., [3, 23–25]). The pulsar-tube radius can either decrease [23] or increase [3].

We estimate here the effect of a circum-pulsar disk on the pulsar-tube radius using the model [23], according to which the magnetic field is given by

$$B_r=\frac{2m}{r^3}\left[\sin\theta\cos\phi\sin\chi+\frac{2}{\pi}\cos\chi\cos\theta\left(\arctan X+\frac{1-Y}{X}\right)\right], \qquad (7)$$

$$B_\theta = \frac{m}{r^3}\Bigg\{ -\cos\theta\cos\phi\sin\chi + \frac{2}{\pi}\cos\chi\sin\theta\Bigg[\arctan X + \frac{\cot^2\theta}{X} \times \left(\frac{YX^2}{\cos^2\theta}\frac{r^2+b^2}{b^2} - 1\right)\Bigg]\Bigg\},$$

$$B_\phi = \frac{m}{r^3}\sin\phi\sin\chi,$$

$$X = b|\cos\theta|\sqrt{2/\left[(r^2-b^2)+r^2/Y\right]},$$
$$Y = r^2/\sqrt{(r^2-b^2)^2+4b^2r^2\cos^2\theta}.$$

Here, all quantities are given in the spherical coordinates (r, θ, ϕ), with the Oz axis directed along the pulsar rotation axis $\mathbf{\Omega}$; b is the inner radius of the disk.

We calculate the pulsar-tube radius as follows. We seek the magnetic lines of force (7) that begin at the points

$$\mathbf{x} = a\left(\mathbf{e}_m\cos\mu + \mathbf{e}_n\sin\mu\right),$$
$$0 \le \mu \le 2\pi,$$

where a is the neutron-star radius, $\mathbf{e}_m = \dfrac{\mathbf{m}}{m}$ is a unit vector along the axis of the main dipole, and $\mathbf{e}_n$ is a unit vector perpendicular to $\mathbf{\Omega}$ and $\mathbf{m}$. For the angle θ_0 denoting the pulsar-tube boundary, we take the value μ corresponding to the last line of force that does not cross the light cylinder.

The effect of an external magnetic field $\mathbf{B}_c$ on the operation of a radio pulsar with a dipolar magnetic field was examined in [26]. To find the pulsar-tube radius, we must seek the magnetic lines of force [26]:

$$\mathbf{B}(\mathbf{r}) = \frac{3(\mathbf{m},\mathbf{r})\mathbf{r} - \mathbf{m}r^2}{r^5} + \mathbf{B}_c. \qquad (8)$$

In the case of axial symmetry, the equation for the lines of force can be found analytically, and the pulsar-tube radius turns out to be [26]

$$d = \sqrt{\frac{1-\alpha_b}{1-\dfrac{\alpha_b}{\eta_{LC}^3}}} \text{ at } \beta = \pi, \chi = 0, \qquad (9)$$

$$d = \max\left(\sqrt[6]{\frac{27}{4}\frac{\alpha_b}{1+\dfrac{\alpha_b}{\eta_{LC}^3}}}, \sqrt{\frac{1+\alpha_b}{1+\dfrac{\alpha_b}{\eta_{LC}^3}}}\right) \qquad (10)$$
$$\text{at } \beta = 0, \chi = 0,$$

where $\eta_{LC} = \left(\dfrac{\Omega a}{c}\right)^{-1}$ is the light-cylinder radius (measured in neutron-star radii), β is the angle between $\mathbf{B}_c$ and the pulsar rotation axis $\mathbf{\Omega}$, $\alpha_b = \dfrac{B_c}{B_0}\left(\dfrac{\Omega a}{c}\right)^{-3}$ (here, $2\alpha_b$ is the ratio of B_c to the magnetic-field intensity of the main dipole at the light cylinder at the tangent point of the last closed line of force).

Formula (9) and the right-hand expression in parentheses in (10) describe the divergence of the magnetic lines of force of (8) at the light cylinder during the formation of a wave zone. The left-hand expression in parentheses in (10) is a special case of the approximation formula from [26]:

$$d = \sqrt[6]{\frac{27}{4}\alpha_b}\left[\cos\left(\frac{\tilde\beta}{2}\right)\right]^{0.48},$$

where $\tilde\beta$ is the angle between $\mathbf{B}_c$ and the direction of the axis of the main dipole $\mathbf{m}$. This formula describes the divergence of the lines of force (their extension to infinity) under the action of a constant external magnetic field. This mechanism is in no way related to the pulsar rotation, and operates even in nonrotating pulsars [26].

4. RESULTS

Figures 1–4 show time-averaged spectra of the gamma-ray radiation of the pulsar tube of a radio pulsar for $B = 0.2B_{\rm cr}$, $P = 0.5$ s, $\chi = 10°$, $k = 0.15$, and $\Delta = 0.1$. The angle between the line of sight and pulsar rotation axis is 10° (i.e., at some time, $\mathbf{m}$ is parallel to the line of sight). The solid curve corresponds to a purely dipolar field ($\nu = 0$), the long-dashed curve to $\nu = 0.1$, the short-dashed curve to $\nu = 0.2$, the dotted curve to $\nu = 0.3$, the dash-dot curve to $\nu = 0.5$, and the dash–double-dot curve to $\nu = 0.7$.

The left-hand graph in Fig. 2 corresponds to the case when the pulsar is surrounded by a circumpulsar disk that cuts the pulsar magnetosphere at a height of one-third of the light cylinder (i.e., $b = 1/3$). The left-hand graphs in Figs. 3 and 4 correspond to the case when the pulsar is in a uniform magnetic field $\mathbf{B}_c$. The magnetic-field intensity B_c is equal to the intensity of the main dipolar field $\mathbf{m}$ at the light cylinder. The left-hand graph in Fig. 3 corresponds to a uniform magnetic field directed opposite to the pulsar rotation axis ($\mathbf{B}_c \uparrow\downarrow \mathbf{\Omega}$); in Fig. 4, this field is aligned with the rotation axis ($\mathbf{B}_c \uparrow\uparrow \mathbf{\Omega}$). Figures 5–7 present parameters of the intensity of the curvature radiation of the pulsar tube as a function of the pulsar phase for the same pulsar.

The table lists the heights of the upper plate z_c and primary-electron energies Γ at the point ($z = z_c, \xi = 0, \phi = 0$) that were used to derive these spectra.

For all cases of a purely dipolar magnetic field ($\nu = 0$) and for non-dipolarity $\nu = 0.1$ with $d = 0.2$,

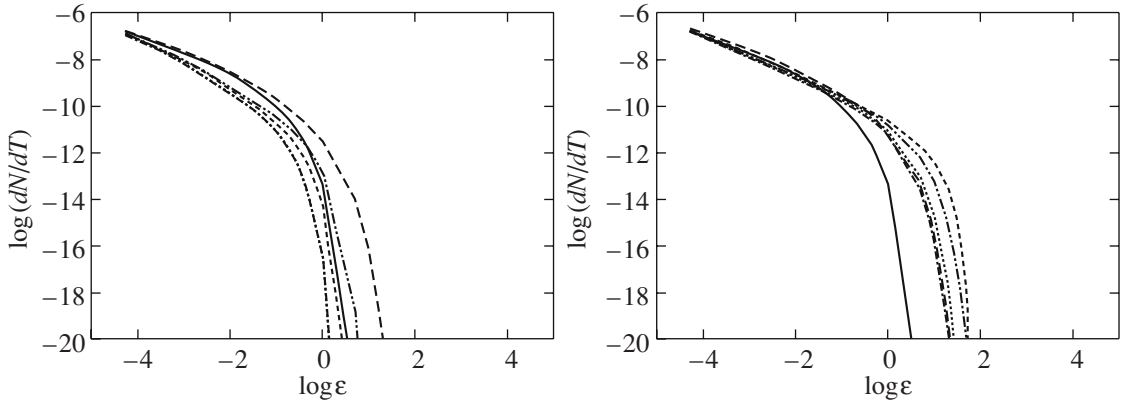

Fig. 1. Time-averaged spectrum of the gamma-ray radiation of a pulsar tube for $B = 0.2B_{\rm cr}$ G, $P = 0.5$ s, $\chi = 10^\circ$, $k = 0.15$, $\Delta = 0.1$, $d = 0.2$, and $\gamma = \pi$ (left), or $\gamma = \dfrac{\pi}{2}$ (right). The solid curve corresponds to a purely dipolar field ($\nu = 0$), the long-dashed curve to $\nu = 0.1$, the short-dashed curve to $\nu = 0.2$, the dotted curve to $\nu = 0.3$, the dash-dot curve to $\nu = 0.5$, and the dash–double-dot curve to $\nu = 0.7$. The gamma-ray intensity $\dfrac{dN}{dt}$ is in units of $\dfrac{\text{photon}}{\text{cm}^2\ \text{s MeV}}$ of the flux received from a source at a distance of 1 kpc. The photon energy ϵ is in MeV. For $\nu = 0$ and $\nu = 0.1$, the lower limit for the gamma-ray intensity is shown: the pulsar is turned off after the creation of electron–positron pairs by curvature radiation in the magnetic field.

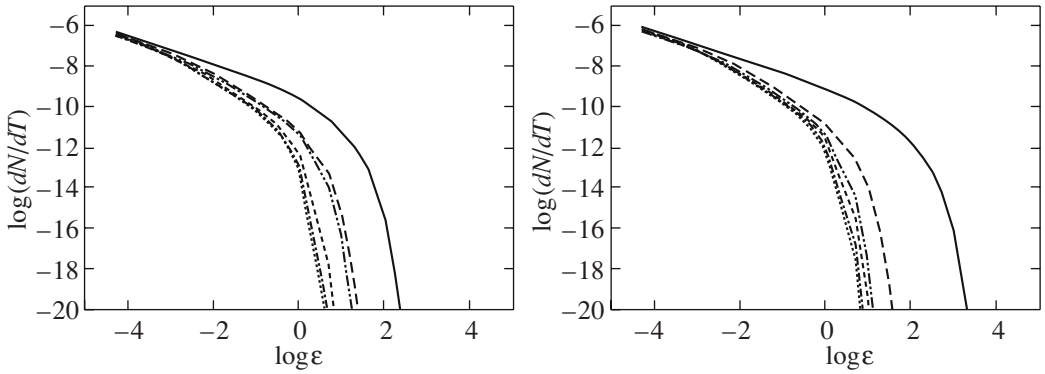

Fig. 2. Same as Fig. 1 for $B = 0.2B_{\rm cr}$ G, $P = 0.5$ s, $\chi = 10^\circ$, $k = 0.15$, $\Delta = 0.1$, $\gamma = \pi$; the left panel coresonds to $d = 0.363$, $\dfrac{\Omega b}{c} = \dfrac{1}{3}$, and the right panel to $d = 0.5$. For the case of a purely dipolar field ($\nu = 0$), the pulsar is turned off.

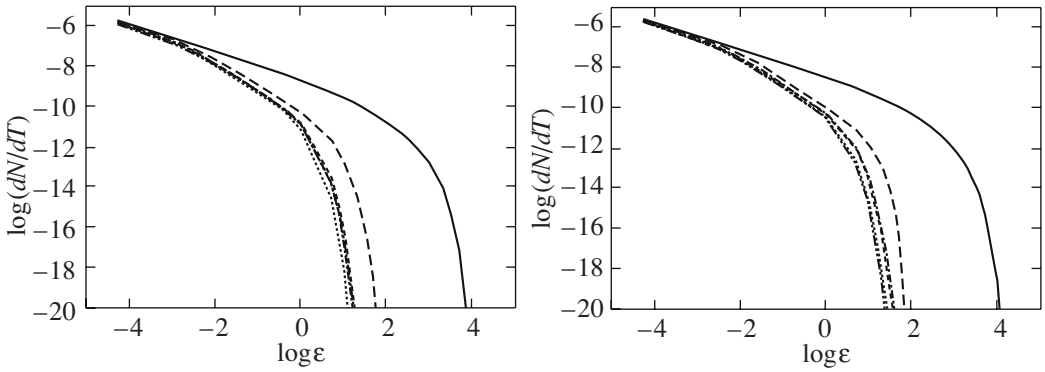

Fig. 3. Same as Fig. 1 for $B = 0.2B_{\rm cr}$ G, $P = 0.5$ s, $\chi = 10^\circ$, $k = 0.15$, $\Delta = 0.1$, $\gamma = \pi$; the left panel corresponds to $d = 0.71$, $\alpha_b = \dfrac{1}{2}$, $\beta = \pi$, and the right panel to the case of an unperturbed pulsar magnetosphere with $d = 1.0$.

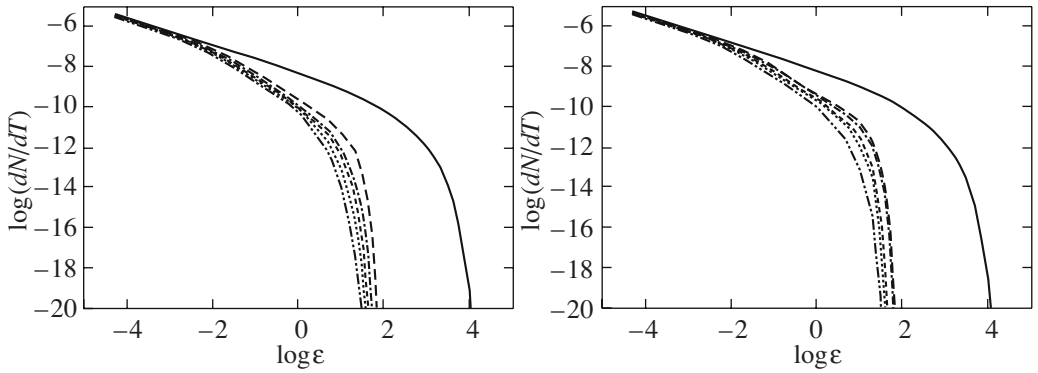

Fig. 4. Same as Fig. 1, for $B = 0.2B_{\rm cr}$ G, $P = 0.5$ s, $\chi = 10^\circ$, $k = 0.15$, $\Delta = 0.1$, $\gamma = \pi$; the left panel corresponds to $d = 1.22$, $\alpha_b = \dfrac{1}{2}$, $\beta = 0$, and the right panel to $d = 1.5$.

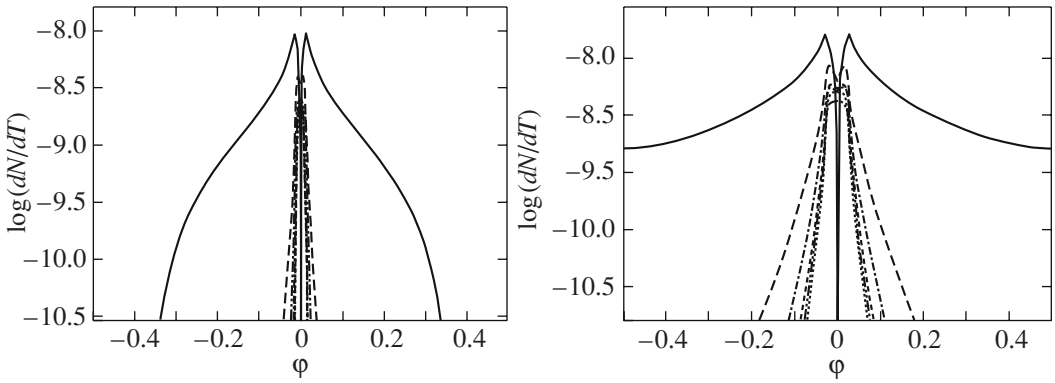

Fig. 5. Pulse shape of the gamma-ray radiation of the pulsar tube for $B = 0.2B_{\rm cr}$ G, $P = 0.5$ s, $\chi = 10^\circ$, $k = 0.15$, $\Delta = 0.1$, and $\gamma = \pi$; the left panel corresponds to $d = 0.5$ and the right panel to $d = 1.0$. The solid curve corresponds to a dipolar field ($\nu = 0$), the long-dashed curve to $\nu = 0.1$, the short-dashed curve to $\nu = 0.2$, the dotted curve to $\nu = 0.3$, the dash-dot curve to $\nu = 0.5$; and the dash–double-dot curve to $\nu = 0.7$. The gamma-ray intensity $\dfrac{dN}{dt}$ is in units of $\dfrac{\text{photon}}{\text{cm}^2\ \text{s MeV}}$ of the flux received from a source at a distance of 1 kpc. The photon energy is 100 keV. Zero phase corresponds to the line of sight being parallel to $\mathbf{m}$. A unit phase increment corresponds to one full revolution of the pulsar.

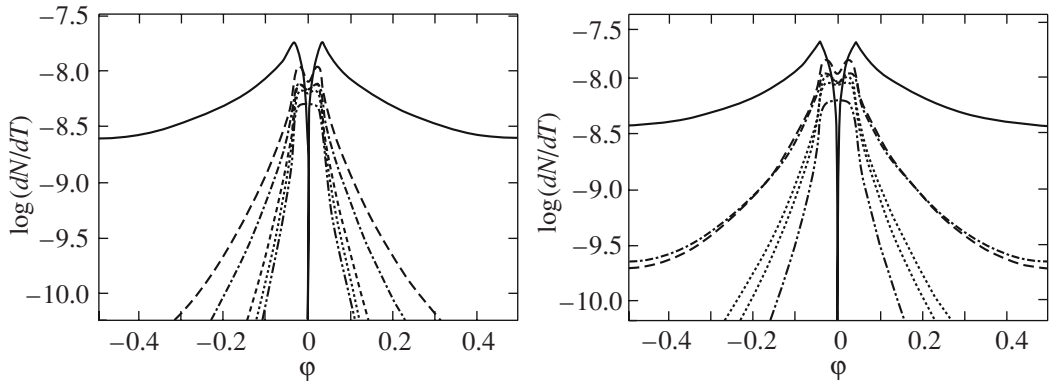

Fig. 6. Same as Fig. 5 for $B = 0.2B_{\rm cr}$ G, $P = 0.5$ s, $\chi = 10^\circ$, $k = 0.15$, $\Delta = 0.1$, and $\gamma = \pi$; the left panel corresponds to $d = 1.22$, $\alpha_b = \dfrac{1}{2}$, $\beta = 0$, and the right panel to $d = 1.5$. The photon energy is 100 keV.

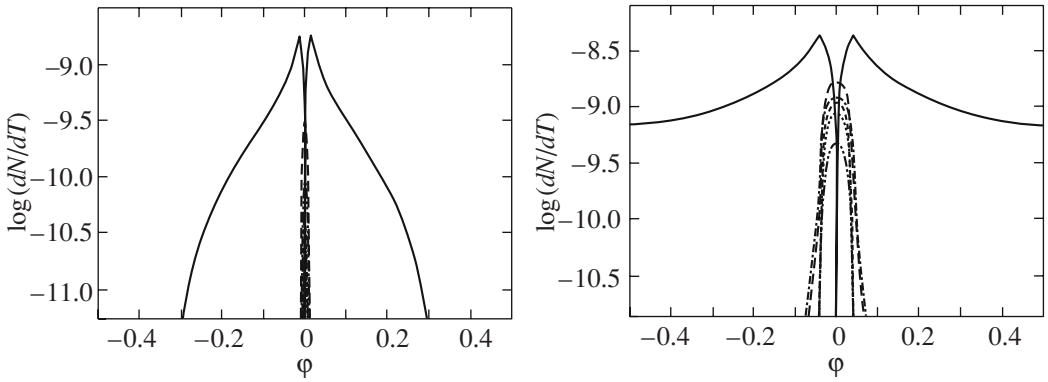

Fig. 7. Same as Fig. 5 for $B = 0.2B_{cr}$ G, $P = 0.5$ s, $\chi = 10°$, $k = 0.15$, $\Delta = 0.1$, and $\gamma = \pi$; the left panel corresponds to $d = 0.5$, and the right panel to $d = 1.5$. The photon energy is 1 MeV.

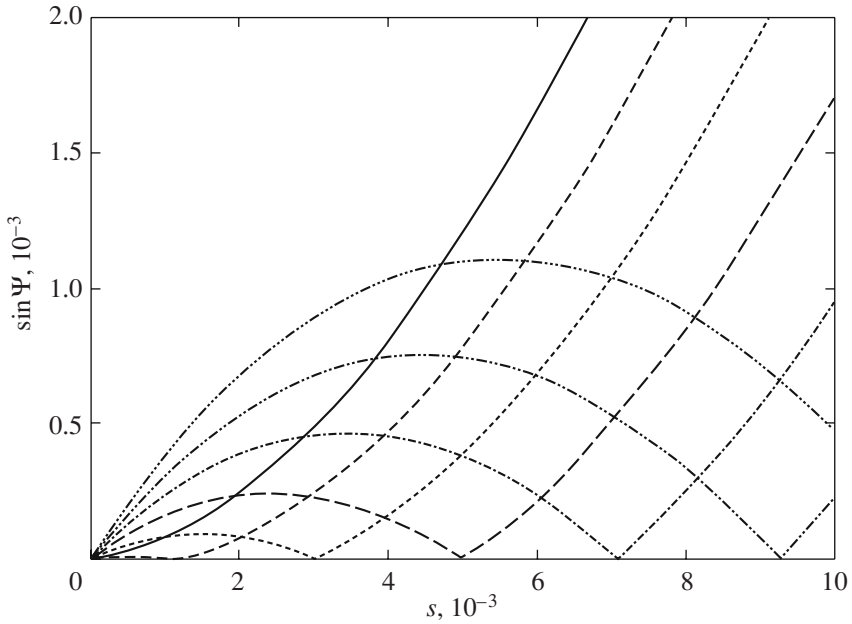

Fig. 8. Angle Ψ between the photon momentum and magnetic field as a function of the path s traversed by the photon. The photon starts from the point $(z = 10^{-2}, \theta, \phi = 0)$. The solid curve corresponds to a starting point with $\theta = 4.0 \times 10^{-2}$, the long-dashed curve to $\theta = 4.1 \times 10^{-2}$, the short-dashed curve to $\theta = 4.2 \times 10^{-2}$, the dotted curve to $\theta = 4.3 \times 10^{-2}$, the dash-dot curve to $\theta = 4.4 \times 10^{-2}$, the dash–double-dot curve to $\theta = 4.5 \times 10^{-2}$, and the dash–triple-dot curve to $\theta = 4.6 \times 10^{-2}$. The parameters of the magnetic field are $B = 0.2B_{cr}$ G, $\nu = 0.6$, and $\Delta = 0.1$. The photon path s is in neutron-star radii.

we used the potential (3) and included radiative deceleration. In all the remaining cases, we used the potential (5) and neglected radiative deceleration.

Figure 1 and the table show that, if the radio pulsar is turned off, the energy of the primary electrons and magnetic-field line curvature grow with the non-dipolarity of the magnetic field. This increases the intensity of the pulsar gamma-ray emission as the non-dipolarity grows (as the pulsar approaches the turn-off limit).

When the pulsar has crossed the turn-off line and has become operational, the upper plate of the pulsar diode appears. This results in a sharp decrease in the potential, as well as the intensity of the gamma-ray emission. Further, we can see from Figs. 2–4 that the intensity of the gamma-ray emission decreases as the non-dipolarity of the magnetic field grows (i.e., as the pulsar moves away from the turn-off line).

However, near $\nu = 0.5$–0.7, we observe a local rise of the potential (and, in some cases, of the height of the upper plate z_c). This results in an increase in the intensity of gamma-ray emission; as a consequence, the average intensity and pulse profile of the pulsar with $\nu = 0.5$–0.7 become very similar to those of a

Heights of the "upper plates" z_c of the diode and primary-electron energies Γ (in units of mc^2) at ($z = z_c$, $\xi = 0$, $\phi = 0$), used to find the gamma-ray intensity for a pulsar with $B = 0.2B_{\rm cr}$ G, $P = 0.5$ s, $\chi = 10^\circ$, $k = 0.15$, $\Delta = 0.1$

ν	z_c, 10^{-2}	Γ, 10^5	ν	z_c, 10^{-2}	Γ, 10^5	ν	z_c, 10^{-2}	Γ, 10^5	ν	z_c, 10^{-2}	Γ, 10^5
$d = 0.2, \gamma = \pi$			$d = 0.2, \gamma = \frac{\pi}{2}$			$d = 0.363, \gamma = \pi, \frac{\Omega b}{c} = \frac{1}{3}$			$d = 0.5, \gamma = \pi$		
0.0	200.0	26.1	0.0	200.0	26.1	0.0	200.0	85.9	0.0	200.0	163.0
0.1	200.0	29.5	0.1	200.0	26.8	0.1	3.21	14.5	0.1	1.93	14.1
0.2	2.72	9.77	0.2	5.21	11.5	0.2	1.31	9.49	0.2	1.12	9.35
0.3	1.54	7.87	0.3	2.23	7.71	0.3	0.94	8.17	0.3	0.85	8.01
0.4	1.15	7.50	0.4	1.50	7.13	0.4	0.78	7.91	0.4	0.72	7.78
0.5	0.98	7.79	0.5	1.21	7.32	0.5	0.70	8.43	0.5	0.66	8.41
0.6	0.94	8.83	0.6	1.10	8.18	0.6	0.70	10.4	0.6	0.67	11.0
0.7	1.05	11.7	0.7	1.16	10.4	0.7	0.73	13.4	0.7	0.61	10.3
0.8	0.79	8.69	0.8	0.98	9.30	0.8	0.54	7.56	0.8	0.50	6.96
$d = 0.71, \gamma = \pi, \alpha_b = \frac{1}{2}, \beta = \pi$			$d = 1.0, \gamma = \pi$			$d = 1.22, \gamma = \pi, \alpha_b = \frac{1}{2}, \beta = 0$			$d = 1.5, \gamma = \pi$		
0.0	45.3	230.0	0.0	15.3	235.0	0.0	9.47	239.0	0.0	6.0	245.0
0.1	1.59	13.5	0.1	1.47	12.9	0.1	1.44	12.6	0.1	1.42	12.5
0.2	1.03	8.99	0.2	1.0	8.74	0.2	0.99	8.73	0.2	1.0	8.88
0.3	0.81	7.76	0.3	0.80	7.72	0.3	0.81	7.85	0.3	0.81	8.15
0.4	0.69	7.64	0.4	0.70	7.80	0.4	0.71	8.08	0.4	0.72	8.61
0.5	0.65	8.48	0.5	0.66	9.03	0.5	0.68	9.79	0.5	0.71	11.3
0.6	0.68	12.4	0.6	0.75	16.8	0.6	0.67	12.5	0.6	0.62	9.65
0.7	0.56	8.62	0.7	0.54	7.63	0.7	0.53	7.22	0.7	0.51	6.86

pulsar with $\nu = 0.1$–0.2. For instance, in the left-hand graph in Fig. 2, the curves corresponding to $\nu = 0.7$ and $\nu = 0.1$ essentially merge; the curves for $\nu = 0.2$, $\nu = 0.5$, and $\nu = 0.7$ in the left-hand graph in Fig. 3 almost coincide; the curves for $\nu = 0.2$, $\nu = 0.5$ and for $\nu = 0.3$, $\nu = 0.7$ in the right-hand graph in Fig. 3 are likewise nearly identical; and the curves corresponding to $\nu = 0.1$ and $\nu = 0.5$ in the right-hand graphs in Fig. 1 and Fig. 4 coincide. Even in this model case, these coincidences severely hinder derivation of the non-dipolarity structure from the intensity of the pulsar gamma-ray emission.

Having passed its maximum, the intensity of the gamma-ray emission again decreases; for example, in the right graph in Fig. 8, the curve for $\nu = 0.7$ lies below the other curves. The presence of a maximum in the dependence of the electrostatic potential on the non-dipolarity is due primarily to the structure of the magnetic field obtained from the model [16] describing the non-dipolarity. In some cases, this structure is such that a photon emitted along the magnetic field $\mathbf{B}$ ($\sin\Psi = 0$, where Ψ the angle between the photon's momentum and $\mathbf{B}$) first acquires a small angle Ψ, then, having traveled some distance, again ends up moving along the magnetic field (i.e., again $\sin\Psi = 0$). Figure 8 shows examples of the acquisition of small angles Ψ by photons starting from different points.

This circumstance strongly hinders the generation of electron–positron pairs near such points (at these heights); this increases the height of the upper plate of the diode z_c, and, consequently, the electrostatic potential.

We must also take into account the fact that the creation of electron–positron pairs is a threshold process ($\gamma \sin\Psi \geq 2$), and, despite the increase in the curvature and potential, the photons still must travel some distance before producing electron–positron pairs. This slows somewhat the decrease in the height of the upper plate of the diode z_c, which makes some (albeit small) contribution to the increase in the electrostatic potential.

Note that the presence and position of a maximum in the potential are very model dependent. For instance, we can see for the cases listed in the table that the maximum gradually shifts from its position at $\nu \sim 0.7$ and $d = 0.2$ to a new position at $\nu \sim 0.5$ and $d = 1.5$ with increasing tube radius.

Moreover, if we determine the height of the upper plate z_c using the condition $Q(z = z_c, \xi = 0, \phi = 0) = 0.1$ instead of (6), this shifts the maximum of the potential by approximately $\delta\nu \sim 0.1$. However, regardless of the method used to find z_c, we observe a gradual shift of the maximum toward smaller values of ν with increasing width d of the pulsar tube.

ACKNOWLEDGMENTS

The authors are grateful to V.D. Pal'shin and A.I. Chugunov for their help with the numerical calculations, to E.M. Kantor, M.E. Gusakov, M.V. Ulanov, Yu.A. Shibanov, and A.A. Danilenko for support and helpful comments, and to A.N. Timokhin for his support. The work was supported by the Program of State Support of Leading Scientific Schools of the Russian Federation (grant no. NSh-9879.2006.2).

REFERENCES

1. A. N. Timokhin, Mon. Not. R. Astron. Soc. **368**, 1055 (2006).
2. A. N. Timokhin, e-Print arXiv:astro-ph/0607165v2 (2006).
3. V. S. Beskin, *Axially Symmetric Stationary Flows in Astrophysics* (Fizmatlit, Moscow, 2006) [in Russian].
4. K. Hirotani and S. Shibata, Mon. Not. R. Astron. Soc. **325**, 1228 (2001).
5. J. A. Hibschman and J. Arons, Astrophys. J. **554**, 624 (2001).
6. A. K. Harding and A. G. Muslimov, Astrophys. J. **556**, 987 (2001).
7. A. K. Harding and A. G. Muslimov, Astrophys. J. **568**, 862 (2002).
8. K. Hirotani, A. K. Harding, and S. Shibata, Astrophys. J. **591**, 334 (2003).
9. A. K. Harding, V. V. Usov, and A. Muslimov, arXiv:astro-ph 0510135v1 (2005).
10. E. T. Scharlemann, J. Arons, and W. M. Fawley, Astrophys. J. **222**, 297 (1978).
11. A. N. Timokhin, G. S. Bisnovatyi-Kogan, and H. C. Spruit, Mon. Not. R. Astron. Soc. **316**, 734 (2000)
12. E. Asseo and D. Khechinashvili, Mon. Not. R. Astron. Soc. **334**, 743 (2002).
13. V. Urpin and J. Gil, Astron. Astrophys. **415**, 305 (2004)
14. J. Gil, G. Melikidze, and B. Zhang, Astrophys. J. **650**, 1048 (2006).
15. V. D. Pal'shin and A. I. Tsygan, Astron. Zh. **73**, 426 (1996) [Astron. Rep. **40**, 385 (1996)].
16. V. D. Pal'shin and A. I. Tsygan, Preprint Phys.-Tech. Institut im. A.F. Ioffe, No. 1718 (FTI Ross. Akad. Nauk, St. Petersburg, 1998).
17. E. M. Kantor and A. I. Tsygan, Astron. Zh. **80**, 665 (2003) [Astron. Rep. **47**, 613 (2003)].
18. D. P. Barsukov, E. M. Kantor, and A. I. Tsygan, Astron. Zh. **83**, 184 (2006) [Astron. Rep. **50**, 159 (2006)].
19. J. Arons and E. T. Scharlemann, Astrophys. J. **231**, 854 (1979).
20. D. P. Barsukov, E. M. Kantor, and A. I. Tsygan, Astron. Rep. **51**, 469 (2007).
21. I. Contopoulos, Astron. Astrophys. **466**, 301 (2007).
22. G. J. Qiao, K. J. Lee, H. G. Wang, et al., Astrophys. J. (Letters) **606**, L49 (2004).
23. J. J. Aly, Astron. Astrophys. **86**, 192 (1980).
24. A. Bardou and J. Heyvaerts, Astron. Astrophys. **307**, 1009 (1996).
25. A. Bardou, Mon. Not. R. Astron. Soc. **306**, 669 (1999).
26. A. I. Tsygan, Mon. Not. R. Astron. Soc. **292**, 317 (1997).

Translated by G. Rudnitskii